Appl. Magn. Reson. (2007) 32, 663–689
DOI 10.1007/s00723-007-0043-y
Printed in The Netherlands

Applied Magnetic Resonance

^{29}Si, ^{27}Al, ^{1}H and ^{23}Na MAS NMR Study of the Bonding Character in Aluminosilicate Inorganic Polymers

M. R. Rowles[1,*], J. V. Hanna[2], K. J. Pike[2,], M. E. Smith[3], and B. H. O'Connor[1]**

[1] Centre for Materials Research, Department of Imaging and Applied Physics, Curtin University of Technology, Bentley, Western Australia, Australia
[2] NMR Facility, Institute of Materials Engineering Science, Australian Nuclear Science and Technology Organisation, Sydney, New South Wales, Australia
[3] Department of Physics, University of Warwick, Coventry, United Kingdom

Received 2 May 2007; revised 12 May 2007

Abstract. ^{29}Si, ^{27}Al, ^{1}H and ^{23}Na solid-state magic-angle spinning (MAS) nuclear magnetic resonance (NMR) has been used to relate nominal composition, bonding character and compressive strength properties in aluminosilicate inorganic polymers (AIPs). The ^{29}Si chemical shift varies systematically with Si-to-Al ratio, indicating that the immediate structural environment of Si is altering with nominal composition. Fast ^{1}H MAS and ^{29}Si $T_{SiH}/T_{1\rho}$ relaxation measurements demonstrated that occluded pore H_2O mobility within the disordered cavities is slow in comparison with H_2O mobility characteristics observed within the ordered channel structures of zeolites. The ^{27}Al MAS NMR data show that the Al coordination remains predominantly 4-coordinate. In comparison with the ^{29}Si MAS data, the corresponding ^{27}Al MAS line shapes are relatively narrow, suggesting that the AlO_4 tetrahedral geometry is largely unperturbed and the dominant source of structural disorder is propagated by large distributions of Si–O bond angles and bond lengths. Corresponding ^{23}Na MAS and multiple-quantum MAS NMR data indicate that Na speciation is dominated by distributions of hydration states; however, more highly resolved ^{23}Na resonances observed in some preparations supported the existence of short-range order. New structural elements are proposed to account for the existence of these Na resonances and an improved model for the structure of AIPs has also been proposed.

1 Introduction

Aluminosilicate inorganic polymers (AIPs), also known as geopolymers [1], have received considerable attention [2–4] in recent years, showing promise in applications such as cements and concretes [5, 6], toxic waste storage [7, 8] and fi-

* Present address: Division of Minerals, CSIRO, Clayton South, Victoria, Australia
** Present address: Department of Physics, University of Warwick, Coventry, UK

ber-reinforced composites [9]. AIPs consist of an amorphous structure resulting from the polymerization of aluminosilicate monomers in an alkaline solution [1]. The amorphous nature of these AIPs makes characterization by techniques for ordered materials, notably X-ray diffraction (XRD), difficult to interpret and elucidate any structural information. To this end, nuclear magnetic resonance (NMR) has been used to elucidate short-range order information regarding the bonding configuration of atoms present in the material. Recent work by Rowles and O'Connor [10] described the influence that chemical composition exercises on the compressive strength of these materials. However, further investigation is needed to establish the link between chemical bonding character and speciation, and compressive strength, to more formally understand the structure–property relationship characterizing AIPs.

One potential use of AIP-type materials is as a replacement for Portland cement. Portland cement concretes are the most extensively used construction material, with approximately 6 billion tonnes being produced annually [11]. Cement manufacturing is one of the leading contributors to world CO_2 production, accounting for 5% of the world's anthropogenic CO_2 output [12]. It is estimated that the use of geopolymer technology could reduce CO_2 emissions from the cement and associated aggregate industries by a factor of five [13]. Another potential application of this class of materials has arisen through investigations into their suitability as immobilization matrices of high-level and low-level nuclear waste from spent nuclear fuel reprocessing and/or weapons production [14–16]. Initial product consistency test (PCT)-type leach testing on Cs and Sr extraction from these systems has demonstrated, at least to a primary suitability stage, that such an application is feasible [17, 18]. To date, little work has been reported on concretes based solely on geopolymers [2, 19–21], as the majority of concrete research has been done on using Portland cements in combination with different geopolymeric ingredients including flyash [22–24], slag [25] and silica fume [26].

Rahier et al. [27–29] proposed the following schematic polymerization reaction for the formation of AIPs by sodium silicate activation of metakaolinite:

$$w\mathrm{Na_2O}\cdot x\mathrm{SiO_2}\cdot y\mathrm{H_2O} + \mathrm{Al_2O_3}\cdot 2\mathrm{SiO_2} \xrightarrow{<100\,^{\circ}\mathrm{C}} w\mathrm{Na_2O}\cdot\mathrm{Al_2O_3}\cdot(2+x)\mathrm{SiO_2}\cdot z\mathrm{H_2O}$$

The values of w, x and y depend on the composition of the alkaline activation solution and z is the degree of hydration of the resultant polymer. While the precise reaction paths are still unknown, Davidovits [1] has proposed reaction pathways involving the polycondensation of hypothetical orthosialate ions, as shown below for two Si-to-Al ratios.

Pathway for AIPs with Si-to-Al molar ratio of 1:1:

$$(\mathrm{Al_2O_3}\cdot 2\mathrm{SiO_2})_{n/2} + 3n\mathrm{H_2O} \xrightarrow{\mathrm{NaOH}} n(\mathrm{OH})_3\text{–Si–O–Al}^{(-)}\text{–}(\mathrm{OH})_3,$$

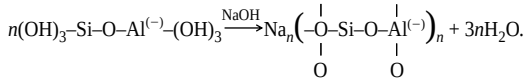

Pathway for AIPs with a Si-to-Al molar ratio of 2:1:

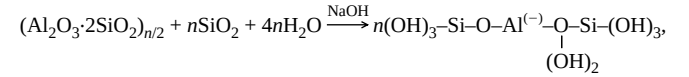

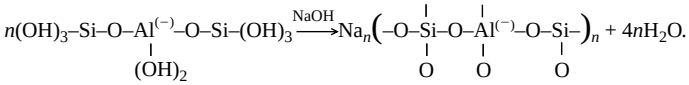

The first reaction pathway shows the production of the polysialate inorganic polymer, with a Si-to-Al ratio of 1, and the second reaction pathway shows the polysialate-siloxo polymer. As additional SiO_2 is added to the system, the siloxo (–Si–O–Si–) chain between the sialate (–SiO–Al–) groups becomes longer.

Solid-state magic-angle spinning (MAS) NMR has been demonstrated to be a very effective tool for characterizing AIPs [30–34]. The technique is able to determine the different coordination environments for every Si, Al and Na position for any given nominal stoichiometric preparation. Furthermore, provided that the preparation is free from paramagnetic species, this information can be quantitative and representative of the bulk sample. Given the typical ranges of coordination of silicon and aluminium in such materials, i.e., silicon is predominately tetrahedral and aluminium can vary between AlO_4, AlO_5 and AlO_6, different factors characterize the change in shift within these materials. In true geopolymers, silicon is present as SiO_4 units that are completely connected (i.e., Q^4; see ref. 25) and it is the number of next-nearest-neighbor aluminium (i.e., $Q^4(m\mathrm{Al})$) that varies, with $m = 0$–4. Since Al is more electropositive than Si, an increase in the number of Al atoms surrounding the SiO_4 unit results in a down-field shift of the ^{29}Si resonance to a less negative position within well-defined chemical shift regions [30, 32, 35–37]. In contrast, an Al coordination number varies more strongly by changing the number of oxygen atoms immediately bonded to each Al position; this number can be 4, 5 or 6. Due to the Loewenstein avoidance principle [38], which asserts that Al–O–Al bonds cannot exist, it is therefore redundant to refer to the number of SiO_4 tetrahedra that can connect to an AlO_n moiety as only silicon can be a next-nearest neighbor. The ^{27}Al chemical shift ranges defining Al^{IV}, Al^{V} and Al^{VI} speciation have been extensively discussed [30, 39]. The ranges are well separated and allow the coordination number of AlO_n units to be unambiguously determined. Unfortunately, the same degree of certainty cannot be obtained from ^{23}Na chemical shifts as the strongly ionic nature of Na^+, and its inability to form bonds with significant covalent character, results in a small overall chemical shift range with ill-defined ^{23}Na shift ranges describing Na speciation. Koller et al. [40] have attempted to map these shift

ranges, but knowledge of the ^{23}Na isotropic chemical shift provides little certainty towards the identification of the Na local environment.

The principal aim of the work presented in this paper is to elucidate changes in the bonding network and speciation as the chemical composition of the AIPs is varied. To address this objective, ^{29}Si, ^{27}Al, ^{1}H and ^{23}Na MAS NMR studies have been undertaken on suites of samples representing a range of compositions in order to give a broad view of the structural variations in the polymer network.

2 Experimental

Three suites of samples with differing chemical compositions were chosen (Table 1 and Fig. 1). Suite A, defined by a fixed Si-to-Na molar ratio (Si:Na = 2), was chosen to give an indication of the change in bonding over the complete Si–Al range as it encompasses both the weakest and strongest samples as measured by compressive strength [10]. Suites B and C consisted of samples that were chosen from the extremities of the composition range to give an indication of the influence of Na-to-Al ratio on the Si-bonding character.

2.1 Raw Materials and Processing

The starting materials were a crystalline kaolinite (Kingwhite 65, Unimin Australia Ltd.) and an amorphous silica fume (Australian Fused Materials Pty Ltd.). Metakaolinite was obtained by heating the kaolinite at 750 °C in air for 24 h, in order to obtain an X-ray amorphous aluminosilicate material with enhanced reactivity to alkaline media [41]. The detailed chemical compositions of the precursor materials are given in ref. 10. All sodium silicate activating solutions were

Table 1. Sample designation, compressive strength and molar composition. The errors given in the compressive strength represent one standard deviation calculated from three samples.

Sample	Suite	Compressive strength (MPa)	Si:Al:Na
Kaolinite	–	–	–
Metakaolinite	–	–	–
Silica fume	–	–	–
1.1/0.6	A	0.40(2)	1.08:1:0.57
1.5/0.8	A	6.2(5)	1.5:1:0.75
2.0/1.0	A	51.3(13)	2.0:1:1.0
2.5/1.3	A	64(3)	2.5:1:1.26
3.0/1.5	A	2.6(2)	3.0:1:1.53
1.1/0.8	B	2.2(3)	1.08:1:0.75
3.0/2.0	B	19.9(7)	3.0:1:2.0
1.1/1.0	C	4.4(7)	1.08:1:1.0
2.0/2.0	C	11.8(16)	2.0:1:2.0

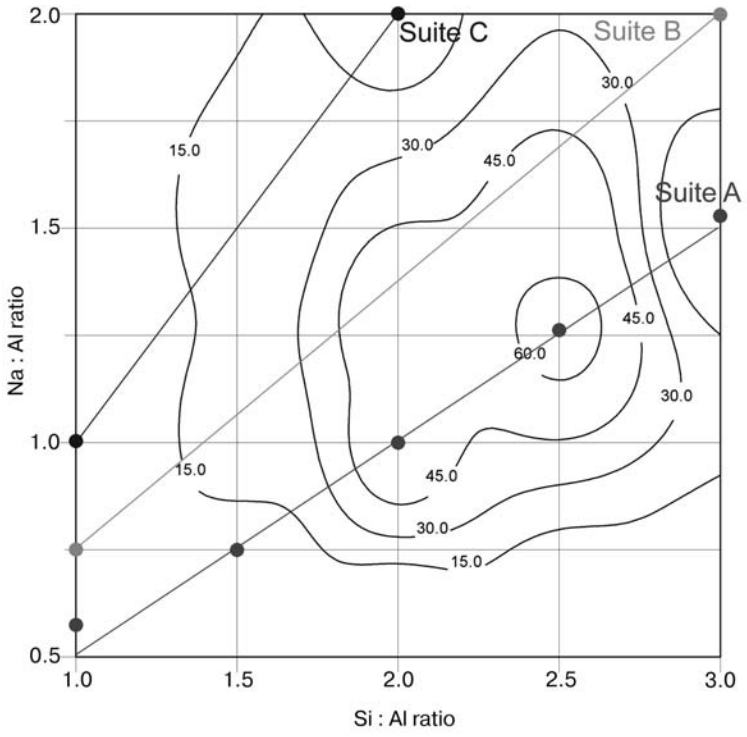

Fig. 1. Contour plot of compressive strength versus compositional Si-to-Al and Na-to-Al molar ratios for the samples under study, from ref. 10. Composition suite A provides a sequence of samples across the composition range, which includes the maximum in compressive strength. Suites B and C provide examples for the extremes of the compositional range.

prepared by mixing the required amounts of sodium hydroxide (Sigma Chemicals Pty Ltd.) and silica fume with deionized water (Si-to-Na molar ratios, 1.0, 1.5 and 2.0; H_2O-to-SiO_2 molar ratios, 2.8) and heating at 75 °C until a clear solution was obtained. No precautions were taken to exclude CO_2 from the solutions. The insoluble zirconia contained in the silica fume was separated from the activating solution by decanting. Samples were prepared with nominal Si-to-Al molar ratios between 1.08–3.0, and with Na-to-Al molar ratios between 0.57–2.0. Water was added to give the final AIP paste the same consistency for all samples. The nominal compositional ratios given in this study are molar ratios unless otherwise explicitly stated, and all AIP samples are identified by their two characteristic ratios of Si to Al and Na to Al (Si:Al/Na:Al).

2.2 MAS NMR Measurements

High-resolution solid-state ^{29}Si and ^{27}Al MAS NMR spectra were acquired at ambient temperatures on an MSL-400 NMR spectrometer ($B_0 = 9.4$ T) operating at

the ^{29}Si and ^{27}Al frequencies of 79.48 and 104.23 MHz, respectively. ^{29}Si MAS NMR data were acquired using a Bruker 7 mm double-air-bearing probe with cross-polarization (CP)MAS and single-pulse (Bloch decay) methods, both of which utilized high-power ^{1}H-decoupling during data acquisition. The MAS frequencies implemented for these measurements were about 5 kHz. For the ^{29}Si CPMAS experiments, a recycle delay of 5 s, a ^{1}H-^{29}Si Hartmann–Hahn contact period of 5 ms and an initial ^{1}H $\pi/2$-pulse width of 5 μs were common to all CPMAS data. For the corresponding ^{29}Si MAS single-pulse high-power ^{1}H-decoupling measurements, a single ^{29}Si $\pi/4$-pulse width of 2.5 μs and a preacquisition delay of 10 μs were used in conjunction with recycle delays of 30–60 s for quantitative ^{29}Si measurements. All ^{29}Si MAS and CPMAS chemical shifts were externally referenced to tetramethylsilane (TMS) at 0 ppm via a high-purity sample of kaolinite (−91.2 ppm) which was also used to establish the ^{1}H-^{29}Si Hartmann–Hahn condition. All ^{27}Al experiments were conducted using a Bruker 4 mm double-air-bearing probe from which MAS frequencies of about 15–16 kHz were implemented for line narrowing, and all measurements utilized single-pulse (Bloch decay) experiments without ^{1}H-decoupling. For quantitative estimates of the central transition intensities to be made, the quadrupolar nature of the ^{27}Al ($I = 5/2$) nucleus necessitated that flip angles are close to the condition [30, 37, 39]

$$(I + 1/2)\omega_{rf}\, t_p \leq \pi/6. \tag{1}$$

For these ^{27}Al measurements, nonselective $\pi/2$-pulse times of 4 μs were calibrated on a 1 M $Al(NO_3)_3$ solution from which selective pulse times of 0.6 μs were employed for data acquisition on all solid samples. Preacquisition delays of 3 μs and relaxation delays of 5 s duration were typical for these measurements; however, checks for abnormally long T_1s were undertaken with recycle delays of up to 30 s being implemented. 1 M $Al(NO_3)_3$ solution was also used as a ^{27}Al chemical shift reference at 0.0 ppm.

High-resolution, variable-temperature, solid-state ^{29}Si MAS data were acquired at 8.45 T on a Varian/Chemagnetics Infinity 360 spectrometer to investigate the magnetization buildup and decay ($T_{SiH}/T_{1\rho}$) characteristics within each geopolymer preparation. All data were acquired using a Varian 6 mm double-air-bearing probe with ^{1}H-excitation pulse and ^{1}H-decoupling conditions similar to those chosen for data acquisition at 9.40 T, with the Hartmann–Hahn contact period being varied typically from 200 μs to 7 ms. For these measurements shorter recycle delays of 1 s were used. Each variable $T_{SiH}/T_{1\rho}$ experiment was performed at 21 and −40 °C to investigate the temperature dependence of the ^{29}Si magnetization dynamics.

High-resolution one-dimensional (1-D) solid-state ^{1}H MAS NMR data were acquired at 14.1 T using a homebuilt, Samoson design, 1.8 mm fast MAS probe. Each ^{1}H spectrum was acquired with a single-pulse-acquire sequence in conjunction with a fast MAS frequency of 40 kHz, a ^{1}H $\pi/2$-pulse time of 2.5 μs, a preacquisition delay of 8 μs and a recycle delay of 120 s. All ^{1}H data are externally referenced to TMS (0.0 ppm) via doubly deionized and distilled H_2O at 4.7 ppm.

High-resolution 1-D solid-state ^{23}Na MAS NMR data were acquired at magnetic field strengths of 8.45, 9.4 and 14.1 T on Varian/Chemagnetics Infinity 360, Bruker MSL-400 and Varian/Chemagnetics Infinity 600 spectrometers operating at characteristic ^{23}Na frequencies of 95.25, 105.10 and 158.74 MHz, respectively. Single-pulse (Bloch decay) ^{23}Na experiments without ^{1}H-decoupling were conducted using Bruker 4 mm double-air-bearing probes at 8.45 and 9.4 T, and a Varian/Chemagnetics 4 mm T3 design probe at 14.1 T, with MAS frequencies in the range of 15–16 kHz. To satisfy the quantitative acquisition conditions described by Eq. (1) for the quadrupolar ^{23}Na ($I = 3/2$) nucleus, nonselective $\pi/2$-pulse times of 3 μs were calibrated on a 1 M NaCl solution from which selective pulse times of 0.6 μs were implemented for data acquisition. The preacquisition delay at each field was 3 μs and the relaxation delays were typically of 8 s duration, with checks for abnormally long T_1s also being undertaken (recycle delays up to 60 s). The 1 M NaCl solution also served as a ^{23}Na chemical shift reference at 0.0 ppm.

^{23}Na 2-D multiple-quantum (MQ)MAS NMR studies [42–45] were performed on a range of AIPs at magnetic field strengths of $B_0 = 8.45$ and 14.1 T on Varian/Chemagnetics Infinity 360 and Infinity 600 spectrometers. An amplitude-modulated triple-quantum (3Q)MAS NMR experiment [42, 46] was used which provided high-resolution hypercomplex 2-D spectra whose indirectly detected dimensions (F_1) have sign discrimination and are free from the second-order quadrupolar broadening exhibited by the central transition of the spin $I = 3/2$ ^{23}Na isotope. At each B_0 field two 2-D MQMAS data sets and a conventional 1-D MAS NMR spectrum using a single-pulse-acquire sequence were acquired for each sample, the latter being used as the F_2 projection for the presented 2-D MQMAS data. All 14.1 T experiments were performed using a Varian 4-mm T3 probe. Each 1-D projection spectrum was acquired with a MAS rate of 15 kHz, and a nonselective $\pi/2$-pulse time of 3.12 μs that was calibrated on solid NaCl which corresponded to a B_1 radiofrequency (rf) field strength of about 80 kHz. A pulse width of 1.0 μs was used for data acquisition (which corresponded to a flip angle of about $\pi/6$), in conjunction with a preacquisition delay of 3 μs and a relaxation delay of 8 s. The 2-D MQMAS studies utilized a MAS rate of 12.5 kHz, with the 3Q-excitation, 3Q-conversion and Z-filter pulses having widths of 4.0, 1.6 and 5.0 μs, respectively. The B_1 field strengths were about 80 kHz for the 3Q-filter pulses and about 20 kHz for the Z-filter pulses. For each sample, relaxation delays of both 6 and 1 s duration were used for the acquisition of all 2-D MQMAS data. The latter experiments exhibited less F_1 resolution, thus focussing on the broader spectral components with faster relaxation rates (as discussed below). Each 2-D MQMAS data set typically required about 4 h for acquisition. Similar experiments were performed at 8.45 T using a Bruker 4 mm rotor probe and a MAS rate of 12.5 kHz. 1-D spectra were acquired with single pulses of 1.0 μs duration with an overall B_1 rf field strength of about 80 kHz again implemented. For the 2-D MQMAS experiments the 3Q-excitation and 3Q-conversion pulses were of 5.0 and 1.9 μs duration, respectively, generated from a B_1 field of about 80 kHz, while the Z-filter pulses were of 4.5 μs duration

from a B_1 field of about 25 kHz. The 8.45 T experiments utilized relaxation delays similar to those performed at 14.1 T (6 and 1 s), but each experiment was typically averaged for twice as many acquisitions.

2.2 Data Analysis

All ^{29}Si and ^{27}Al chemical shifts, integrated intensities and line widths from the data presented in Figs. 2 and 3 were measured by the WINFIT profile fitting software [47]. Chemical shifts (δ) and line widths were extracted from these simulations; however, the reported ^{27}Al shift positions do not represent isotropic chemical shifts as they remain uncorrected for second-order quadrupolar effects [30, 37, 39], unless otherwise stated.

Each ^{29}Si and ^{27}Al spectrum was simulated five times, with the average of these data reported in Table 2 as chemical shifts and line widths. An example of the curve fitting procedure used to calculate the peak positions and line widths is given in Fig. 4. For the ^{29}Si and ^{27}Al spectra of the inorganic poly-

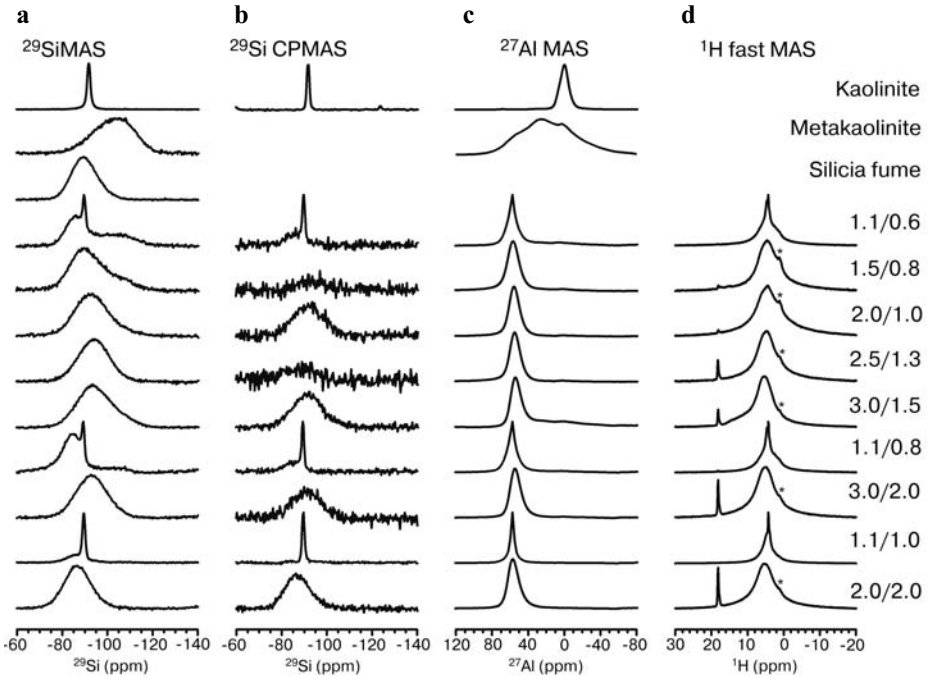

Fig. 2. Measured ^{29}Si MAS data (**a**), ^{29}Si CPMAS data (**b**), ^{27}Al MAS data (**c**) and ^{1}H fast MAS data (**d**) for the range of AIP compositions under study. In the ^{1}H MAS data, the resonance at 18.1 ppm is assigned to HCO_3^- resulting from small amounts of sample hydrolysis and carbonation, while the less resolved resonance at about 1.0 ppm (asterisk) is a background artifact due to the organic polymer rotor cap material.

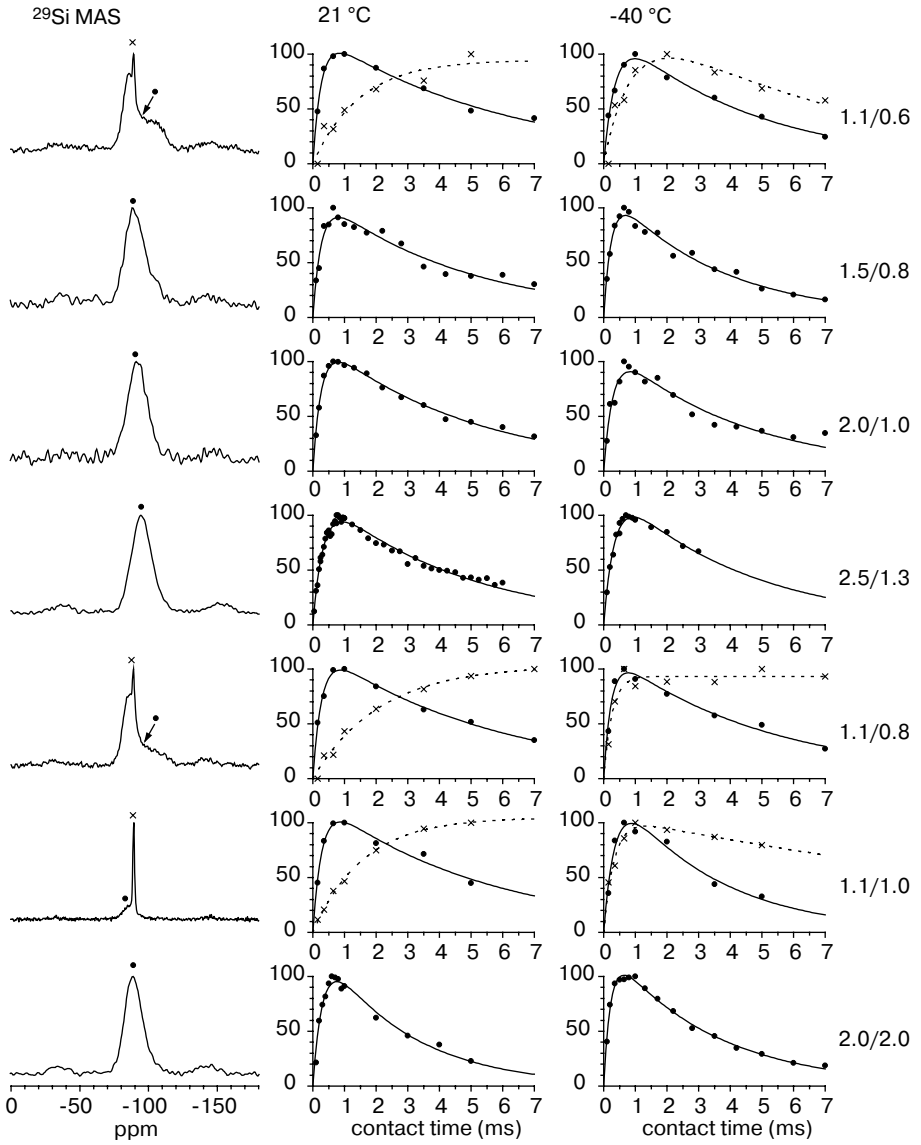

Fig. 3. ^{29}Si $T_{SiH}/T_{1\rho}$ variable contact time experiments as performed for the entire suite of AIP preparations. The ^{29}Si shift positions at which this behavior is measured is indicated for the AIP (●) and zeolite (x) components.

mers, the values for the chemical shift and line width for metakaolinite were fixed, and only the resonance area was refined. The change to relative speciation of each sample was elucidated from the change in these fitted spectral regions. All errors quoted are two standard deviations of the mean, calculated

Table 2. Reported ^{29}Si and ^{27}Al chemical shifts, line widths and ^{29}Si CP period time constants of the nominal compositions composing suites A, B and C and associated precursor materials.

Sample	Suite	^{29}Si						^{27}Al	
		δ_{iso} ±0.1 (ppm)	Line width ±0.02 (kHz)	T_{SiH} ±0.02 21 °C (ms)	$T_{1\rho}$ ±0.02 21 °C (ms)	T_{SiH} ±0.02 −40 °C (ms)	$T_{1\rho}$ ±0.02 −40 °C (ms)	δ ±0.1 (ppm)	Line width ±0.01 (kHz)
Kaolinite	–	−91.7	0.11[a]					0.0	1.05
								1.6	5.38
Metakaolinite	–	−104.8	1.64					29.1	3.56
								53.6	2.17
Silica fume	–	−111.4	1.11					–	–
1.1/0.6	A	−85.8	0.84	0.27	6.03	0.40	4.34	58.3	1.04
		−89.7[b]	0.11	1.47[b]	−[c]	1.00[b]	6.95[b]		
1.5/0.8	A	−88.9	1.18	0.28	4.67	0.26	3.43	56.5	1.60
2.0/1.0	A	−92.1	1.26	0.28	4.85	0.32	4.12	55.3	1.38
2.5/1.3	A	−94.0	1.26	0.35	4.50	0.37	4.20	54.6	1.40
3.0/1.5	A	−92.8	1.32					56.2	1.13
1.1/0.8	B	−84.4	0.78	0.29	5.59	0.26	5.02	58.2	1.04
		−89.4[b]	0.11	2.11[b]	−[c]	0.26[b]	−[c]		
3.0/2.0	B	−92.9	1.27					55.5	1.06
1.1/1.0	C	−86.5	0.84	0.30	5.26	0.40	3.13	57.4	0.55
		−89.5[b]	0.12	1.58[b]	− [c]	0.34[b]	16.80[b]		
2.0/2.0	C	−85.9	1.17	0.35	2.71	0.24	3.29	58.0	1.12

[a] This represents a total line width which is composed of two crystallographically inequivalent positions; each resolved resonance (observed under appropriate ^{1}H-decoupling conditions) contributes a width of about 50–55 Hz to the total line width at 9.4 T.
[b] Measurement of zeolite A component within this preparation.
[c] Not measured.

from the fivefold simulation of each spectrum. The coordination numbers for the different Si and Al structural moieties composing each AIP were ascertained by directly comparing all measured ^{29}Si and ^{27}Al chemical shifts with well-established ^{29}Si and ^{27}Al chemical shift ranges that have been reported for aluminosilicate, cementitious and siliceous materials [30, 37, 39]. The notation describing Si and Al coordination environments is consistent with that employed by Lippmaa et al. [35, 37] and Engelhardt et al. [32].

3 Results and Discussion

The ^{29}Si, ^{27}Al and ^{1}H MAS NMR data are shown in Figs. 2 and 3, and the corresponding variable B_0 ^{23}Na data are given in Figs. 6 and 8 (see below). Table 2 provides the corresponding ^{29}Si and ^{27}Al chemical shifts, line widths, and the measured T_{SiH} and $T_{1\rho}$ time constants characterizing the competing processes responsible for the buildup and decay of the ^{29}Si magnetization within these systems.

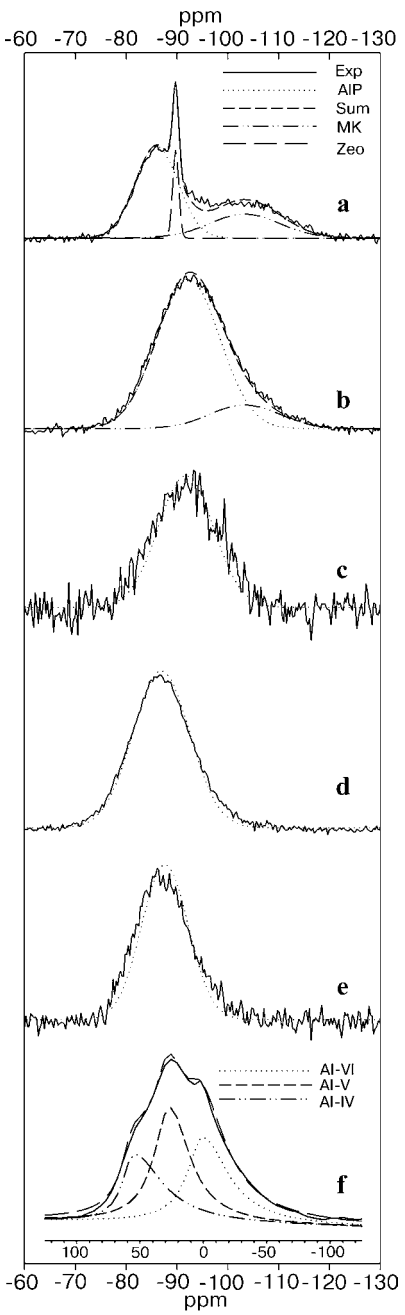

Fig. 4. Examples of the spectral simulation and deconvolution of ^{29}Si and ^{27}Al MAS data used to calculate chemical shifts, line widths and relative intensities for sample 1.1/0.6, ^{29}Si MAS (**a**), sample 2.0/1.0, ^{29}Si MAS (**b**), sample 2.0/1.0, ^{29}Si CPMAS (**c**), sample 2.0/2.0, ^{29}Si MAS (**d**), sample 2.0/2.0, ^{29}Si CPMAS (**e**), and metakaolinite, ^{27}Al MAS (**f**).

3.1 ^{29}Si and ^{1}H MAS NMR Studies

The kaolinite spectrum in Fig. 2a exhibits a characteristic single narrow ^{29}Si resonance positioned at −91.5 ppm, indicating a classic Q^3 Si species in a highly ordered matrix with no chemical shift dispersion [30, 32, 48–50]. An expansion of this spectrum (not shown) indicates that very highly crystalline kaolinite samples devoid of paramagnetic impurities can exhibit two partially resolved resonances with very similar chemical shifts if the high-power ^{1}H-decoupling field strength is of sufficient intensity. In contrast, metakaolinite and silica fume show very broad resonances at −104.8 ppm (Q^4(1Al)–Q^4(0Al)) and −111.5 ppm (Q^4), respectively, which are indicative of highly disordered structural networks. Since the nearest-neighbor interactions influence the chemical shift of a particular Si species, the shift of the ^{29}Si resonance from kaolinite to that of metakaolinite suggests that the Si network is becoming detached from the Al network; i.e., Al is exerting less influence on the Si chemical shift and the Si sublattice in metakaolinite is tending towards that observed for silica fume.

Upon accurate spectral simulation of the quantitative ^{29}Si MAS NMR data in Fig. 2a, the AIPs exhibit chemical shifts ranging between −85.5 and −94.0 ppm. In terms of the next-nearest-neighbor aluminium coordination number (*m*) in Q^4(*m*Al), the ^{29}Si chemical shifts correlate to a variation in *m* of about 3.7–2.2, as estimated from an interpolation of established literature values [30, 32, 35, 36]. A plot of *m* versus sample composition for suite A is shown in Fig. 7a, and it reflects a reduction in *m* from about 3.7 for sample 1.1/0.6 (Si:Al/Na:Al) (−85.8 ppm) to a value of about 2.2 for sample 2.5/1.3 (−94.0 ppm). (The estimated errors in the silicon-to-aluminium coordination number *m* in Fig. 7a take account of the ^{29}Si chemical shift spread associated with each coordination num-

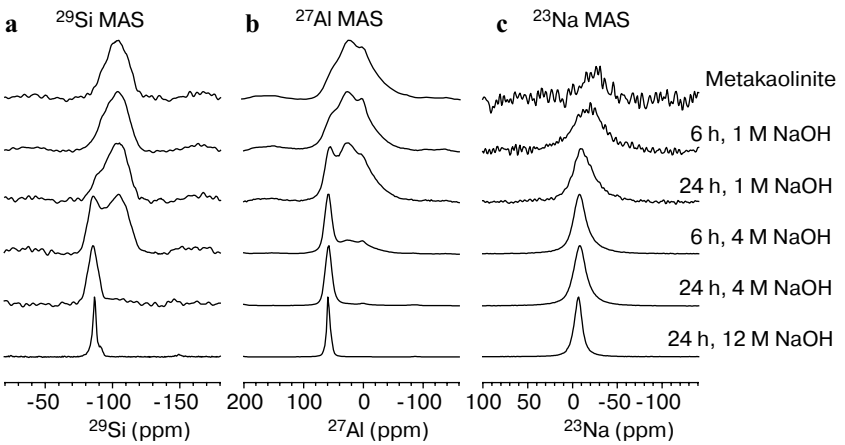

Fig. 5. ^{29}Si MAS (**a**), ^{27}Al MAS (**b**) and ^{23}Na MAS data (**c**) for the reaction of metakaolinite precursor with varying-strength NaOH for different time periods, without stoichiometric adjustment from Na silicate solutions.

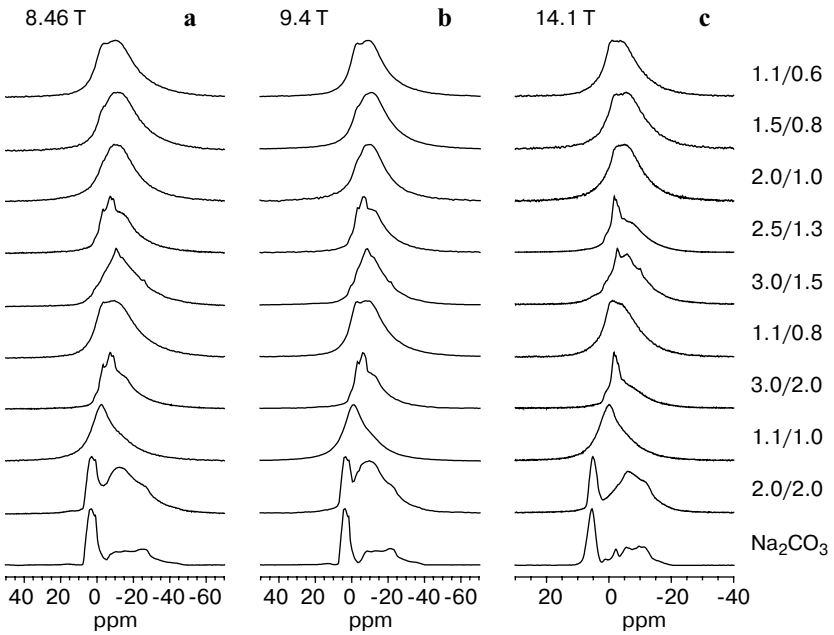

Fig. 6. ^{23}Na MAS NMR data for the entire AIP suite acquired at 8.45 T (**a**), 9.4 T (**b**), and 14.1 T (**c**). Data for Na_2CO_3 is included for comparative purposes to demonstrate its influence on some data.

ber and were calculated as two standard deviations of the average of the chemical shift values reported for sodium aluminosilicate systems [30, 32, 35, 36].) Furthermore, this shift in the resonance position, and the concomitant change in Si coordination, is mirrored by the physical properties of the material. The compressive strength of the AIPs shown in Fig. 7b increases to a maximum at sample 2.5/1.3 and then decreases rapidly and monotonically on either side of the compositional range, directly correlating with the amount of residual unreacted metakaolinite coexisting in each final product. From Fig. 7b it can be observed that maximum compressive strength is achieved when undetectable levels of metakaolinite are observed in the highest strength 2.5/1.3 preparation. Residual unreacted metakaolinite is readily observed in the ^{29}Si MAS spectra of Fig. 2 as a semiresolved higher-field tail situated at about -105 ppm, which is an unambiguous match with the spectrum of the metakaolinite precursor also shown in Fig. 2. Some typical examples of the spectral deconvolution and simulation methods employed to ascertain the amounts of the metakaolinite residues within these data are shown in Fig. 4a and b. Metakaolinite and other unreacted precursor residues within AIP preparations have also been reported by other authors [17, 18, 28]. This additional inhomogeneity can influence the strength of the AIP in two ways: firstly, it can act as flaws in the bulk polymer structure thus promoting cracks and fractures to propagate through the bulk material, and secondly, the presence of substantial quantities of metakaolinite alters the nomi-

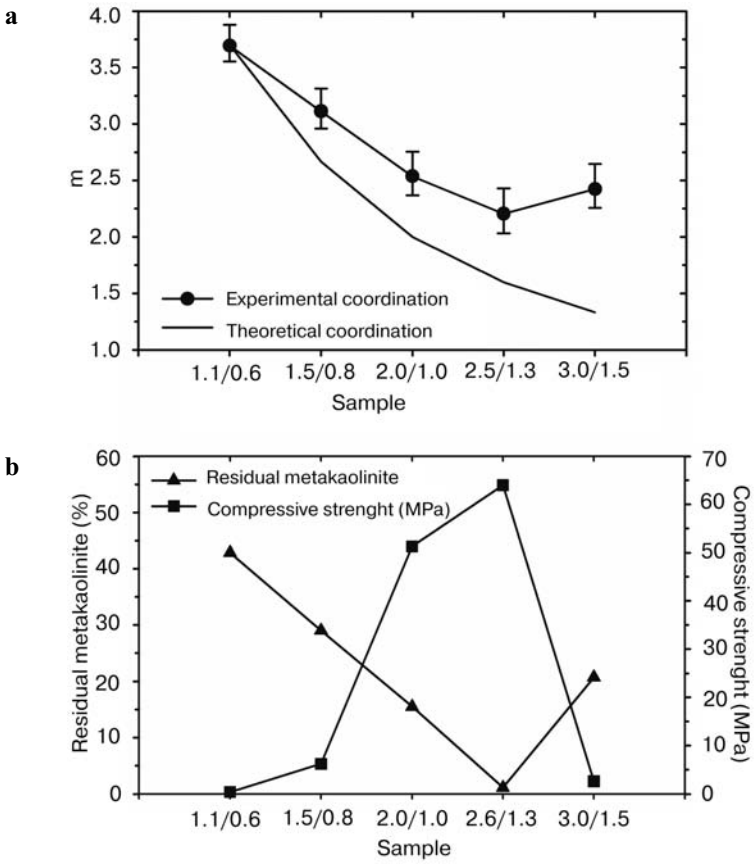

Fig. 7. a Variation of the parameter *m* describing the Si next-nearest Al neighbor coordination ($Q^4(mAl)$) versus sample composition. The upper plot shows the variation in *m* coordination calculated from the measured chemical shift. The lower plot shows the theoretical coordination number assuming the polymer network is made of solely SiO_4 and AlO_4 tetrahedra, with no residual unreacted metakaolinite accounted for. **b** Relative atomic percent concentrations of residual unreacted metakaolinite present in the AIP compositions of suite A as calculated from the ^{29}Si MAS spectra, correlated with their compressive strength characteristics.

nal composition of the AIP relative to the bulk stoichiometry, which may inhibit the complete development of the polymer network.

From Fig. 7a it can be observed that the Si coordination to next-nearest Al neighbors *m* derived from the ^{29}Si chemical shifts differs from the theoretically derived *m* values calculated from the nominal Si-to-Al ratio which assumes the complete dissolution of metakaolinite. The theoretical *m* values derived from these nominal compositions assume that the polymer network is composed entirely of SiO_4 and AlO_4 tetrahedra. The deviation in *m* value between the observed and theoretical trends of Fig. 7a implies that the Al content of the AIP is higher than

what is possible according to the nominal sample composition, suggesting that other factors such as the Na content of the AIP may be affecting the dependence of ^{29}Si chemical shift on the calculated coordination number. One prospective mechanism for this effect is that some Na is being incorporated into the AIP network as a $–SiO^{-}(Na^{+})–Si–$ moiety, thus altering (reducing) the number of SiO_4 tetrahedra directly bonded to the reference SiO_4 tetrahedron. The consequence of Na creating an altered Q^4 Si species of this type may invoke a downfield shift of the ^{29}Si resonance, in similar fashion to having an electropositive next-nearest Al neighbor, subsequently inflating the apparent Al content. This behavior mirrors the previously reported growth of calcium aluminosilicate polymer networks in glasses through the formation of –Si–O–Ca– linkages [51].

For samples 1.1/0.6, 1.1/0.8 and 1.1/1.0 a narrow resonance situated at about −89.4 to −89.7 ppm is observed in both the ^{29}Si MAS and CPMAS spectra, indicating the presence of an ordered second phase through zeolite formation. Previously reported XRD analyses [52] revealed that zeolite A is the preferentially formed ordered phase occurring from these nominal compositions (Linde type A zeolite [53]). The extent of this zeolite formation was measured from the deconvolution and simulation of the ^{29}Si MAS data which were acquired under quantitative conditions (see Fig. 4a). Within these preparations this additional component is estimated as 1.1/0.6 (6.8 w/w%), 1.1/0.8 (7.1 w/w%) and 1.1/1.0 (45 w/w%). It is interesting to observe that no evidence of zeolite formation was detected in sample 2.0/2.0 by either ^{29}Si MAS or CPMAS NMR, even though small amounts of poorly formed zeolite A were detected by XRD studies [52]. This notable absence suggests that under the formation conditions of this zeolite component within sample 2.0/2.0, the resolution and intensity afforded by this phase is insufficient for detection despite the fact that this sample composition resides on the edge of the zeolite formation region. The ^{29}Si MAS NMR line widths of these AIPs range between 0.78 and 1.3 kHz, (i.e., about ten times the width of crystalline kaolinite), indicating that the Si environment in these preparations is amorphous. These line widths are distributed into two distinct groups; the AIP formulations that support zeolite formation exhibit line widths in the range of 0.78–0.84 kHz, whereas samples not bearing any zeolite content exhibit broader line widths of 1.2–1.3 kHz. This bimodal distribution suggests that any zeolite present in the material modifies the development of the AIP network. Depending on the distribution of the zeolite crystals, the zeolite could act as a pinning center, thus assisting the AIP network formation from becoming increasingly disordered. A series of well-distributed crystallites would continuously interrupt the development of the AIP structure and could act as a template which would serve to modify the AIP structure over several bond lengths as the aluminosilicate changes from a zeolite to an AIP.

As noted in previous ^{29}Si MAS and CPMAS studies of AIPs [14], the corresponding data of Figs. 2a, 2b and 3 demonstrate that under typical ^{1}H-^{29}Si CP experimental settings (i.e., contact period about 2–5 ms, recycle delay about 2–10 s) a significant signal decrease is observed with the implementation of the CPMAS technique in comparison with single-pulse methods. Even though typi-

cal H_2O contents of the as-synthesized AIPs reside within a 20–35 w% range [8, 14], the resulting high ^{1}H-concentration alone is insufficient to produce a sensitivity enhancement. From Fig. 2a and b it is observed that the AIP ^{29}Si signal intensity is more severely affected than the zeolite component present in some of the AIP preparations; in such cases the influence of thermal motion on the heteronuclear ^{1}H-^{29}Si spin decoupling process has to be considered. Theoretical treatments of this problem predict that insufficient thermal averaging coupled with the (typically) inefficient heteronuclear decoupling field strengths implemented on systems exhibiting motional correlation times (τ_c) in these regimes render the line broadening to be unmanageable and high-resolution data of the rare (^{29}Si) spins cannot be acquired [32, 54]. In an analogous manner, the fast ^{1}H MAS spectra of Fig. 2d demonstrate that the ^{1}H line widths of all the AIPs are far broader than those of any zeolite component; although chemical shift dispersion is a small contribution to this observation, this phenomenon is dominated by the very different T_2s characterizing these systems, thus indicating that the H_2O mobility in the ordered zeolite channels is far more rapid than that displayed by the occluded H_2O trapped in the disordered pores of the AIP network. In this case, the fast ^{1}H MAS experiment is much more efficient in removing any residual homonuclear ^{1}H–^{1}H dipolar interactions in situations where rapid H_2O mobility is already modulating a large portion of this interaction (i.e., in the zeolite cases), and it is less effective as a line-narrowing technique when it is dealing with much larger residual ^{1}H–^{1}H dipolar interactions in the AIP systems where the H_2O mobility is slow.

The variable contact time $T_{SiH}/T_{1\rho}$ data of Fig. 3 and Table 2 are consistent with these observations. Irrespective of AIP nominal composition, the measured T_{SiH} values fall in a narrow range of about 0.27–0.35 ms, which is approximately an order of magnitude shorter than the corresponding T_{SiH} values of about 1.47–2.11 ms measured for the zeolite A components of samples 1.1/0.6, 1.1/0.8 and 1.1/1.0. Furthermore, from this short T_{SiH} behavior, the optimum contact period that should be adopted for CP signal enhancement appears to be about 1 ms, and this is very consistent across the entire AIP range demonstrating that the heteronuclear ^{1}H–^{29}Si dipolar interaction facilitating the Hartmann–Hahn contact in the CP experiment is much stronger in the AIPs where the restricted H_2O mobility is present. Additionally, the corresponding AIP $T_{1\rho}$ values of about 2.71–6.03 ms are similarly short, indicating that an efficient spin–lattice relaxation mechanism exists. This contrasts markedly from the zeolite cases where, over the contact time range employed in this study, the $T_{1\rho}$ measurements were unable to be determined as the very slow magnetization increase via the T_{SiH} mechanism is dominating an even slower $T_{1\rho}$ relaxation mechanism. A further contrast in H_2O mobility characteristics, and subsequent heteronuclear ^{1}H-^{29}Si dipolar coupling strengths, between the AIP and zeolite systems is emphasized when the temperature of the variable contact experiment is reduced from ambient temperatures (21 °C) to −40 °C. For the AIP case, the $T_{SiH}/T_{1\rho}$ characteristics remain largely invariant over this temperature range, whereas the zeolite T_{SiH}s and $T_{1\rho}$s reduce markedly to the ranges of about 0.24–1.00 ms and about 6.95 and

16.8 ms, respectively, thus demonstrating an increasing strength of the ^{1}H-^{29}Si dipolar characteristics through reduced mobility. The general relaxation behavior of these AIP systems appears to be dominated by a dipolar mechanism with the characteristic motional τ_c values clustering around the intermediate T_1 minimum/T_2 plateau regime where both relaxation processes are fast and $T_1 \approx T_2$ [32, 54]. Although the ^{1}H T_1s become very short, this property cannot be fully exploited as this motional regime is incompatible with CP dynamics and heteronuclear dipolar decoupling processes as mentioned above. Quick checks of the ^{1}H T_1 relaxation at 8.45 T (21 and −40 °C) and at 14.1 T (both not shown) demonstrate that these T_1s are under 0.2 s.

Rahier et al. [28] reported that their ^{29}Si MAS NMR data were invariant with changes in the Si-to-Al ratio, and that samples synthesized with Na-to-Al ratios exceeding stoichiometric values (Na:Al = 1) showed silicate resonances in addition to the AIP resonance. These resonances disappeared after washing, indicating that they were due to excess Na silicate in the activating solution. In contrast to the Rahier study [28], the present study has shown that the ^{29}Si spectra change systematically when the Si-to-Al ratio is altered, and that no Na silicate peaks were present in any of the AIP formulations. The method of sample preparation via creation of a sodium silicate solution adopted by Rahier et al. [28] was closely followed in this study; however, there were differences in the curing methods that were undertaken. Their curing practice employed the use of a closed mould at room temperature for at least two days, while the sample curing method adopted in this study [10] involved the use of similar closed moulds at an elevated temperature of 75 °C. The fundamental differences in the ^{29}Si MAS NMR data are ascribed to the different curing methods employed, thus emphasizing that the production method can profoundly affect the chemical, microstructural and physical properties exhibited by these materials.

3.2 ^{27}Al MAS NMR Study

In Fig. 2c the ^{27}Al MAS spectrum of crystalline kaolinite shows a single resonance characterized by an uncorrected ^{27}Al shift of −0.01 ppm (at 9.4 T) and a line width of 1.05 kHz, indicating the presence of an ordered Al^{VI} species [39, 55]. A detailed variable B_0 field analysis of kaolinite shows that there is a considerable second-order quadrupolar contribution to this line width and that the apparent ^{27}Al shifts are very field-dependent, with an isotropic chemical shift (δ_{iso}) of 8.0 ppm being reported [39]. In contrast, the highly disordered metakaolinite precursor material exhibits three broader resonances at 53.6, 29.1 and 1.6 ppm (elucidated via spectral simulation, see Fig. 4f), which are assigned to Al^{IV}, Al^{V} and Al^{VI} coordination environments, respectively [56]. These resonances exhibit larger line widths in the range of 2.2–5.4 kHz. From this deconvolution the relative percentages of these Al^{IV}, Al^{V} and Al^{VI} coordination environments composing the metakaolinite precursor are estimated to be about 10%, 34% and about 56%, respectively. The multiple coordination environments and amorphous na-

ture of metakaolinite enhances the reactivity of the material and initiates the polymerization reaction [57].

The ^{27}Al MAS NMR data for the entire suite of AIPs is dominated by a single resonance exhibiting an apparent uncorrected shift in the 54.5–58.5 ppm range suggesting a complete (or near complete) transformation under high pH conditions from the Al distributions encountered in the metakaolinite bulk material to only Al^{IV} speciation. A vertical expansion of the baseline of these data (not shown) indicates that very minor contributions of Al^{V} and Al^{VI} are evident which correspond to the presence of residual unreacted metakaolinite, as supported by the ^{29}Si MAS data. This is most apparent in samples 1.1/0.6, 1.5/0.8 and 3.0/1.5. From initial observations of the ^{29}Si and ^{27}Al MAS data in Figs. 2a, c and 4b there appears to be some discrepancy in the amount of unreacted metakaolinite detected by these experiments. As reported above, the deconvolution of the ^{29}Si MAS data accurately measures the unreacted metakaolinite content to be the order of about 20–40% (see Fig. 7b), whereas similar deconvolution of the corresponding ^{27}Al MAS data (at best) reliably estimates a reduced presence in only some of these samples (see Table 3). For example, the ^{29}Si MAS spectrum of sample 1.5/0.8 predicts that about 30% of the measured signal intensity is due to residual metakaolinite; however, the Al^{V} and Al^{VI} resonances in the corresponding ^{27}Al MAS spectrum only account for about 5% of that measured total intensity. To investigate these observations further, NaOH-activated metakaolinite has been studied without any further stoichiometric adjustment with sodium silicate solutions. In these cases, the effects of metakaolinite exposure to variable-strength NaOH (i.e., changing pH) for different time periods are observed, as an analogue for incompletely mixed or inhomogeneous portions of an AIP preparation. The results of this simplified system are shown in Fig. 5, and two conclusions can be drawn. Firstly, for certain combinations of time and pH, the evolution of Al speciation to Al^{IV} appears to be more rapid and detectable than the concomitant transformation in the ^{29}Si network to the sodalite-type structures. This is particularly evident during the initial stages of the metakaolinite activation and is clearly highlighted by the case of metakaolinite exposure to 4 M NaOH for 6 h within Fig. 5. From this observation it could be inferred that all residual metakaolinite in the total suite of AIPs has altered from its initial state as a precursor. Secondly, any speciation transformation from highly distorted,

Table 3. Estimated levels of Al present in samples according to coordination number.

Sample	Al(IV) ± 2 (%)	Al(V) ± 2 (%)	Al(VI) ± 2 (%)
Metakaolinite	10	34	56
1.1/0.6	69	6	25
1.5/0.8	95	0	5
2.0/1.0	98	0	2
2.5/1.3	98	0	2
3.0/1.5	59	12	29

metastable Al^{V} and Al^{VI} environments can produce ^{27}Al resonances with excessively large line widths [30] which are characterized by quadrupole coupling constants (C_Qs) of over 15 MHz. These very broad resonances will not be adequately narrowed and sampled with MAS rates of about 15–16 kHz at 9.4 T and may be acutely underestimated. These systems require more extensive investigation with fast MAS at higher fields, coupled with a more rigorous treatment of the spectral simulation and associated satellite contributions, to reliably quantify Al speciation characterized by a very large range of C_Q values [30, 39, 58].

An important observation of these ^{27}Al MAS data is that the measured line widths of these AIP spectra at 9.4 T lie within the range of about 0.6–1.6 kHz. From Table 2 it is clear that the narrower ^{27}Al line widths of about 0.6–1.0 belong to samples 1.1/0.6, 1.1/0.8 and 1.1/1.0 possessing large zeolite A contributions. Hence, the majority of the AIP suite without additional zeolite components exhibit line widths in a more representative (reduced) range of about 1.0–1.6 kHz, which is very comparable to that observed for crystalline kaolinite. From this result it can be inferred that some degree of short-range order exists within the Al^{IV} positions of the AIP network. In similar fashion to the kaolinite resonance, the ^{27}Al AIP resonances have a second-order quadrupolar contribution to their line widths as evidenced by the very small extended tailing on the upfield side of each line shape, which indicates that only minor distributions within δ_{iso} and C_Q are influencing the width and shape of these resonances [59–62], and that the AlO_4 tetrahedral geometry is largely unperturbed. This contrasts markedly with the ^{29}Si MAS data which describes these systems as being highly disordered, where there is over an order of magnitude difference between the line widths observed for kaolinite and the AIPs (see Table 2). The disparity between the structural descriptions reflected by the ^{27}Al and ^{29}Si MAS data implies that the short- and long-range structural disorder throughout the AIP network is mainly propagated through large distributions of bond angles and bond lengths about the Si positions only. A structural description of this nature is consistent with the pathway for AIP formation (Si-to-Al molar ratio, 2:1) proposed in Sect. 1, where the formation of a polysialate-siloxo polymer possessing additional siloxo (–Si–O–Si–) linkages between the sialate (–Si–O–Al–) moieties could promote this type of partitioned disorder.

3.3 ^{23}Na MAS NMR Study

The conventional single-pulse ^{23}Na MAS NMR data that were acquired at magnetic field strengths of 8.45, 9.4 and 14.1 T are shown in Fig. 6. The corresponding 2-D MQMAS data acquired at 8.45 and 14.1 T are given in Fig. 8. From Figs. 6 and 8 it is quite evident that straightforward homogeneous Na speciation does not exist throughout a large proportion of the nominal compositions studied. A close inspection of the variable field spectra of Fig. 6 reveals that the line widths decrease with increasing B_0, and that the apparent shifts move to lower field, thus converging on the true ^{23}Na isotropic chemical shift δ_{iso},

indicating that a substantial second-order quadrupolar contribution to the line width of these ^{23}Na resonances exists.

The dominant ^{23}Na resonance observed across the suite of AIP preparations is a broad featureless line shape that occurs at an apparent shift of about 5 ppm. Very little information describing the nature the Na speciation can be ascertained from these 1-D data except that the majority of Na in each sample resides in disordered environments similar to those experienced in glass systems. The 2-D MQMAS data are more informative, showing contours that appear skewed in specific directions depending on the applied magnetic field strength. The 2-D MQMAS data acquired at 14.1 T exhibits contours that are predominantly skewed at about 60° to the conventional isotropic chemical shift axis, i.e., along the chemical shift distribution axis [43, 63]. Hence, the MQMAS data at this higher field indicate that a significant distribution of isotropic chemical shifts (δ_{iso}) contribute to this broad inhomogeneous resonance. In contrast, the 2-D MQMAS data acquired at the lower field of 8.45 T emphasize more prominently the quadrupolar contribution to these ^{23}Na line widths in comparison with that experienced at 14.1 T. Figure 8 illustrates that these 8.45 T contours have altered to reflect a predominant skewing at about −50° along the quadrupolar distribution axis [43, 63], thus indicating that a substantial distribution in ^{23}Na quadrupolar parameters is also induced by this structural disorder. Both 8.45 and 14.1 T MQMAS data sets are represented with more clarity when shorter relaxation delays are employed, implying that the Na species represented by these broad inhomogeneous resonances have shorter T_1 relaxation characteristics in comparison with other spectral components that may also exist. Although the apparent shifts for these broad resonances occur at about 5–10 ppm (depending on B_0), the true isotropic chemical shift (δ_{iso}) will be located further downfield at about 0 ppm. This evidence suggests that the broad resonance represents hydrated Na^+ ions in the pore water and void spaces within the AIP network, and the distributions described above represent actual variations in the hydration state of each solvated Na^+ ion and size distributions of the occupied void spaces where these hydrated species reside.

For samples with nominal compositions reflecting an excess Na content (i.e., 2.0/2.0), Figs. 6 and 8 show that a prominent field-dependent resonance at about −5 ppm is observed. In these preparations the Na speciation is dominated by extraneous Na_2CO_3 and $NaHCO_3$ which is not formally incorporated into the AIP network. Unambiguous evidence of this assignment can be elucidated from both the 1-D and 2-D data of Figs. 6 and 8, and from the prominent HCO_3^- resonance at 18.1 ppm in the ^{1}H fast MAS data of Fig. 2d. A comparison of the ^{23}Na MAS spectra of anhydrous Na_2CO_3 at each field with that from the 2.0/2.0 sample (see Fig. 6a, b and c) shows that an excellent correlation with the downfield resonance at about −5 ppm is observed. Furthermore, this comparison shows that a large portion of the much broader ^{23}Na resonance centered about 5 ppm, which is associated with the AIP network, is also part of the total Na_2CO_3 spectrum. These second-order-broadened quadrupolar resonances attributed to Na_2CO_3 narrow markedly with increasing B_0; however, their line shapes are not well-defined. Since the dominant room temperature form (the γ polymorph) shows an

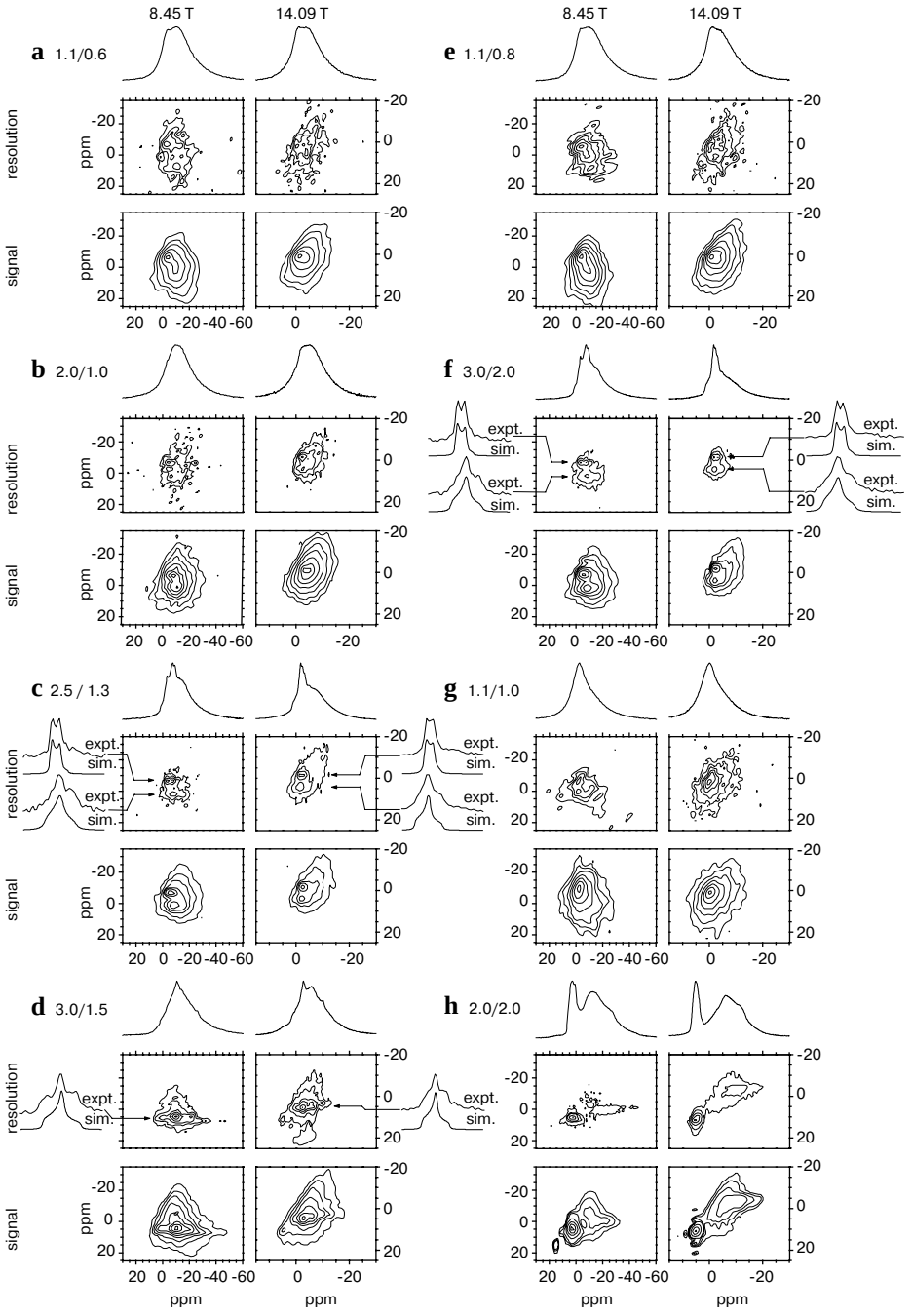

Fig. 8. ^{23}Na 2-D MQMAS data for the entire AIP suite acquired at 8.45 and 14.09 T. At each field, long recycle delay (6 s) experiments focussing on more highly resolved components with slower T_1 relaxation, and short recycle (1 s) experiments focussing on broader components with faster T_1 relaxation, were acquired.

incommensurate structure [64], some degree of structural disorder is inherent; in addition, there is the possibility that some hydrated variants of Na_2CO_3 may coexist with $NaHCO_3$, thus creating a mixture of phases. From Fig. 8h the 2-D MQMAS data from this sample clearly distinguishes the ^{23}Na narrower downfield resonance at each field and in both the long- and short-relaxation forms of the experiment. In addition, the long-relaxation experiment at 8.45 T also resolves (via T_1 discrimination) the broader (i.e., larger C_Q) site at the expense of observation of the remainder of the total AIP Na speciation. These observations are in agreement with previous studies utilizing ^{23}Na MQMAS detection of Na_2CO_3 impurities in $NaHCO_3$ systems upon hydrolysis and carbonation [65].

In addition to the broad dominant ^{23}Na resonance described above, Figs. 6 and 8 illustrate that additional Na species can also be detected. These are characterized by narrower resonances superimposed upon the broad dominant AIP bulk ^{23}Na resonance, with apparent shifts in the range of about 0–5 ppm. Furthermore, these species exhibit distinct second-order quadrupolar structure and much longer T_1 characteristics. In particular, the 1-D ^{23}Na MAS data reported in Fig. 6 for the high Si content AIP preparations 2.5/1.3, 3.0/1.5 and 3.0/2.0 show that these additional components are quite prominent. A study of the corresponding 2-D MQMAS data from Fig. 8 further resolves these species from that of the AIP bulk. For samples 2.5/1.3 and 3.0/2.0 the MQMAS data reveals that two additional Na moieties exist, both of which appear to exhibit second-order quadrupolar structure and δ_{iso} values close to 0 ppm. The extraction of the slices parallel with the F_2 (or anisotropic MAS) dimension shown on Fig. 8c and f confirms that clearly defined second-order quadrupolar broadened resonances are observed at both fields. From these ^{23}Na subspectra, and the pronounced B_0 field dependence exhibited by them, line shape simulation yields values of δ_{iso}, C_Q and the asymmetry parameter (η) with reasonable accuracy. One resonance is characterized by the parameters $\delta_{iso} = 0.0 \pm 0.5$ ppm, $C_Q = 1.35 \pm 0.05$ MHz and $\eta = 0.22 \pm 0.1$, while the other exhibits the following characteristics: $\delta_{iso} = 2.0 \pm 0.5$ ppm, $C_Q = 1.6 \pm 0.1$ MHz and $\eta = 0.9 \pm 0.1$. Figure 8d shows that only the latter type of Na species is evident in sample 3.0/1.5.

The appearance of such line shapes further verifies that some degree of short-range order is present within certain structural components within the AIP network corroborating the findings reflected by the ^{27}Al MAS NMR studies. It is important to note that these high Si content AIPs are far removed from the nominal composition regime that defines the low Si content preparations such as 1.1/1.0, 1.1/0.8 and 1.1/0.6, which are prone to concomitant zeolite A crystallization, as evidenced by XRD studies [52] and by the absence of crystalline phases in the ^{29}Si MAS NMR. Hence, these ^{23}Na resonances describing some degree of short-range order cannot be ascribed to zeolite formation.

3.4 Proposed Structural Models

The AIP structural models presented by Barbosa et al. [31], Davidovits [66] and Li [67] refer to the polymer network as being constructed of SiO_4 and AlO_4 tet-

rahedra, and that the Na^+ charge-balancing cation is present in cagelike structures in the polymer. Davidovits [66] and Li [67] further associate the Na cation directly with AlO_4 tetrahedra, although no mention is made of how the Na is structurally incorporated. The cavities shown in the structural model of Barbosa et al. [31] suggest that Na is present solely in a hydrated form. The data presented in this current study shows that Na is present in a range of hydrated states and sometimes shows short-range order, which suggests that the role of Na solely as a charge-balancing cation is understating its purpose and that it may be active in forming and modifying the polymer network.

As mentioned above, the major component of network disorder in these AIPs is generated by large distributions of bonding characteristics associated with the Si positions, while the AlO_4 tetrahedra remain largely unperturbed. While there is no question that the bulk of the Na speciation resides within various hydration states of Na^+ ions within the pore water, the notion of short-range order can be introduced through different modes of Na interaction with specific framework segments. As demonstrated by the ^{23}Na MAS NMR data, this appears most prevalent with high Si content preparations. In situations where sufficient OH^- is present and able to interact with the cavity structure, surface-bound Na aluminate moieties such as the structure proposed in Fig. 9a are possible and would be consistent with the lower η line shape at $\delta_{iso} = 0.0 \pm 0.5$ ppm ($C_Q = 1.35 \pm 0.05$ MHz, $\eta = 0.22 \pm 0.1$) observed in Fig. 8c and f. Similar Na aluminate-type structures have been observed to form as quasistable intermediates in the acid hydrolysis of high pH aluminate solutions during the polymerization and eventual condensation reactions to form gibbsite [68, 69]. For situations where OH^- is not directly involved or accessible, Na may associate with siliceous parts of the framework to form $–SiO^-(Na^+)–Si–$ moieties, as depicted in Fig. 9b. In this case it is proposed that the net negative charge from AlO_4 tetrahedral units would become localized on the bridging O atoms thus forming $–Si–O^–Si–$ intermediate, which would subsequently stimulate an ionic association with Na^+ ions to stabilize this type of framework structure. The consistent appearance of a higher η line shape at $\delta_{iso} = 2.0 \pm 0.5$ ppm ($C_Q = 1.6 \pm 0.1$ MHz, $\eta = 0.9 \pm 0.1$) in high Si content AIPs (see Fig. 8c, d and f) could be rationalized with this type of short-range order. The formation of both of these proposed short-range order species potentially accounts for the discrepancy between the observed and theoretical behavior of m (see Fig. 7a) characterizing the degree of next-nearest-neighbor Al occupancy (i.e., $Q^4(m\text{Al})$) for the Si speciation. In addition, these proposed structures exist without inducing substantial network termination and concomitant sample degradation. It is interesting to note that for this suite of AIPs, the superior compressive strength performance was displayed by sample 2.5/1.3, which exhibits both forms of these proposed short-range order species. This observation is consistent with improved strength and hardness properties in materials such as glass ceramics which are achieved by the promotion of ordered microdomains formed during the quenching and cooling stages of preparation [70–73].

In light of these propositions, an improved structural model (as depicted in Fig. 9c) is proposed for AIP polymerization and formation from an NaOH-activated metakaolinite precursor approach. It incorporates all of the structural

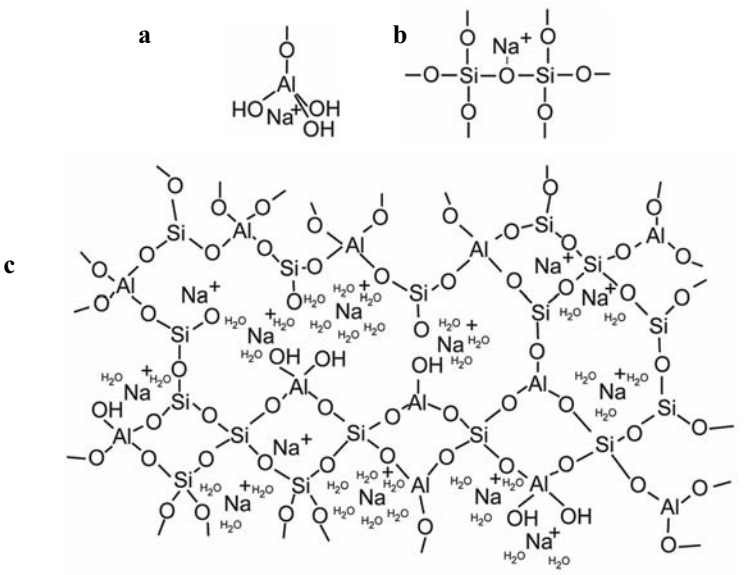

Fig. 9. a Proposed model for the location of the charge-balancing Na^+ cation which assumes the form of a semiattached Na aluminate species. **b** Proposed model for the location of the charge-balancing Na^+ cation which assumes the form of a modified bridging network. **c** Proposed schematic model for AIP structure based on an original model by Barbosa et al. [31] but which attempts to incorporate the new elements mentioned above.

elements discussed above and it acknowledges that aspects of previously proposed models are still valid. From this study it is evident that the initial nominal composition of each AIP is critical in dictating the structural speciation and the physical properties displayed by these materials, and that any proposed model needs to be specific to that type of preparation.

4 Conclusion

The use of the multinuclear MAS NMR technique for the systematic study of a suite of AIP compositions has provided valuable insights into the physical and structural aspects of AIP chemistry and mechanical performance. Each of the nuclei involved (^{29}Si, ^{27}Al, ^{1}H and ^{23}Na) allows quite different aspects of the AIP network to be investigated. Of primary importance is the observation that, for a systematic suite of AIP preparations of known composition, the ^{29}Si chemical shift is sensitive to the changing nature of the bulk network, irrespective of whether other phases such as zeolites and metakaolinite are present. The systematic variation of the ^{29}Si chemical shift is able to be directly correlated with compressive strength properties and the overall $Q^4(m\mathrm{Al})$ coordination of the Si. Fast ^{1}H MAS and ^{29}Si $T_{\mathrm{SiH}}/T_{1\rho}$ relaxation measurements have demonstrated that occluded pore

H_2O mobility within the disordered cavities is slow in comparison to H_2O mobility characteristics observed within the ordered channel structures of zeolites. This leads to much stronger homonuclear ^1H–^1H and heternonuclear ^1H–^{29}Si dipolar bound systems as evidenced by the larger residual line widths in the ^1H MAS data and the very short T_{SiH} and $T_{1\rho}$ relaxation times characterizing the AIP systems, in comparison with corresponding measurements of ordered zeolite frameworks. Furthermore, the insensitivity of the relaxation measurements to temperatures in the range of 21 to −40 °C supports these observations. In contrast to the ^{29}Si MAS studies, the corresponding ^{27}Al data suggest that less disorder exists about the AlO_4 structural units in comparison to what is propagated through the AIP network by disorder in Si–O bond lengths and angles. This is a fundamental feature of the AIP network. The different estimations of unreacted metakaolinite as measured by the ^{29}Si MAS and ^{27}Al MAS experiments suggests that Al transformation from Al^V and Al^{VI} to Al^{IV} species is more rapid than overall Si transformation, at least for the early stages of metakaolinite activation. Finally, the ^{23}Na 1-D and 2-D MAS data clearly show that different types of Na species can be observed, ranging from highly disordered hydration states to proposed elements of short-range order involving structural aspects of the framework. The presence of these newly proposed Na species can be rationalized with the measured disparity between the observed and theoretical behavior of the parameter m characterizing the degree of next-nearest-neighbor Al occupancy describing $Q^4(m\text{Al})$ Si speciation. Most importantly, they are not associated with any form of a network termination process that would facilitate the degradation of the AIP physical properties; these newly proposed Na species are most readily observed in preparations exhibiting superior compressive strength performance. From these many facets of structural information, an improved model of a typical AIP network is proposed.

Acknowledgments

M.R.R. acknowledges receipt of an Australian Postgraduate Award scholarship and an Australian Institute of Nuclear Science and Engineering (AINSE) Post-Graduate Research Award. J.V.H. acknowledges the funding of AINSE project 02/189. M.E.S. thanks Engineering and Physical Sciences Research Council and the University of Warwick for funding NMR equipment.

References

1. Davidovits, J.: J. Therm. Anal. **35**, 429–441 (1989)
2. Palomo, A., Grutzeck, M.W., Blanco, M.T.: Cem. Concr. Res. **29**, 1323–1329 (1999)
3. van Jaarsveld, J.G.S., van Deventer, J.S.J., Lorenzen, L.: Miner. Eng. **10**, 659–669 (1997)
4. Allahverdi, A., Skvára, F.: Ceram. Silik. **45**, 81–88 (2001)
5. Roy, D.M.: Cem. Concr. Res. **29**, 249–254 (1999)
6. Shi, C., Stegemann, J.A.: Cem. Concr. Res. **30**, 803–808 (2000)
7. van Jaarsveld, J.G.S., van Deventer, J.S.J., Schwartzman, A.: Miner. Eng. **12**, 75–91 (1999)

8. Perera, D.S., Blackford, M.G., Vance, E.R., Hanna, J.V., Finnie, K.S., Nicholson, C.L., in: Hanchar, J.M., Stroes-Gascoyne, S., Browning, L. (eds.) MRS Proceedings – Scientific Basis for Nuclear Waste Management XXVIII, vol. 824, pp. 607–612. Materials Research Society, Warrendale (2004)
9. Lyon, R.E., Balaguru, P.N., Foden, A., Sorathia, U., Davidovits, J., Davidovics, M.: Fire Mater. **21**, 67–73 (1997)
10. Rowles, M., O'Connor, B.: J. Mater. Chem. **13**, 1161–1165 (2003)
11. Sabir, B.B., Wild, S., Bai, J.: Cem. Concr. Compos. **23**, 441–454 (2001)
12. Worrell, E., Price, L., Martin, N., Hendriks, C., Meida, L.O.: Annu. Rev. Energy Environ. **26**, 303–329 (2001)
13. Davidovits, J.: World Resour. Rev. **6**, 263–278 (1994)
14. Blackford, M.G., Hanna, J.V., Pike, K.J., Vance, E.R., Perera, D.S.: J. Am. Ceram. Soc. **90**, 1193–1199 (2007)
15. Zosin, A.P., Priimak, T.I., Avsaragov, K.B.: Atom. Energy **85**, 510–514 (1998)
16. Khalil, M.Y., Merz, E.: J. Nucl. Mater. **211**, 141–148 (1994)
17. Perera, D.S., Vance, E.R., Aly, Z., Davis, J., Nicholson, C.L.: Ceram. Trans. **176**, 91–96 (2006)
18. ASTM Committee C26, Standard Test Methods for Determining Chemical Durability of Nuclear, Hazardous, and Mixed Waste Glasses and Multiphase Glass Ceramics: The Product Consistency Test. ASTM, Philadelphia (2000)
19. Alonso, S., Palomo, A.: Mater. Lett. **47**, 55–62 (2001)
20. Moulin, E., Blanc, P., Sorrentino, D.: Cem. Concr. Compos. **23**, 463–469 (2001)
21. Davidovits, J., Davidovits, M., Davidovits, N.: Process for Obtaining a Geopolymeric Alumino-Silicate and Products Thus Obtained. US patent 5342595, 1994.
22. Wong, Y.L., Lam, L., Poon, C.S., Zhou, F.P.: Cem. Concr. Res. **29**, 1905–1913 (1999)
23. Shehata, M.H., Thomas, M.D.A.: Cem. Concr. Res. **30**, 1063–1072 (2000)
24. Fan, Y., Yin, S., Wen, Z., Zhong, J.: Cem. Concr. Res. **29**, 467–472 (1999)
25. Pereira, D.A., Aguiar, B.D., Castro, F., Almeida, M.F., Labrincha, J.A.: Cem. Concr. Res. **30**, 1131–1138 (2000)
26. Lam, L., Wong, Y.L., Poon, C.S.: Cem. Concr. Res. **28**, 271–283 (1998)
27. Rahier, H., Simons, W., van Mele, B., Biesemans, M.: J. Mater. Sci. **32**, 2237–2247 (1997)
28. Rahier, H., van Mele, B., Biesemans, M., Wastiels, J., Wu, X.: J. Mater. Sci. **31**, 71–79 (1996)
29. Rahier H., van Mele, B., Wastiels, J.: J. Mater. Sci. **31**, 80–85 (1996)
30. MacKenzie, K.J.D., Smith, M.E.: Multinuclear Solid-State Nuclear Magnetic Resonance of Inorganic Materials. Pergamon, London (2002)
31. Barbosa, V.F.F., MacKenzie, K.J.D., Thaumaturgo, C.: Int. J. Inorg. Mater. **2**, 309–317 (2000)
32. Engelhardt, G., Michel, D.: High-Resolution Solid-State NMR of Silicates and Zeolites. Wiley, Chichester (1987)
33. Duxon, P., Fernanez-Jiminez, A., Provis, J.L., Luckey, G.C., Palomo, A., van Deventer, S.J.: J. Mater. Sci. **42**, 2917–2973 (2007)
34. Brew, D.R.M., MacKenzie, K.J.D.: J. Mater. Sci. **42**, 3990–3993 (2007)
35. Lippmaa, E., Mägi, M., Samoson, A., Tarmak, M., Engelhardt, G.: J. Am. Chem. Soc. **103**, 4992–4996 (1981)
36. Nofz, M., Engelhardt, G., Wihsmann, F.-G., Forkel, K., Mägi, M., Lippmaa, E.: Z. Chem. **26**, 221–222 (1986)
37. Lippmaa, E., Samoson, A., Mägi, M.: J. Am. Chem. Soc. **108**, 1730–1735 (1986)
38. Loewenstein, W.: Am. Miner. **39**, 92–96 (1954)
39. Smith, M.E.: Appl. Magn. Reson. **4**, 1–64 (1993)
40. Koller, H., Engelhardt, G., Kentgens, A.P.M., Sauer, J.: J. Phys. Chem. **98**, 1544–1551 (1994)
41. Murat, M.: Cem. Concr. Res. **13**, 511–518 (1983)
42. Brown, S.P., Wimperis, S.: J. Magn. Reson. **128**, 42–61 (1997)
43. Fernandez, C., Amoureux, J.P.: Chem. Phys. Lett. **242**, 449–454 (1995)
44. Medek, A., Harwood, J.S., Frydman, L.: J. Am. Chem. Soc. **117**, 12779–12787 (1995)
45. Frydman, L., Harwood, J.S.: J. Am. Chem. Soc. **117**, 5367–5368 (1995)
46. Amoureux, J.-P., Fernandez, C., Steuernagel, S.: J. Magn. Reson. **123**, 116–118 (1996)
47. Krumm, S.: Winfit, ver: 1.2.1, 1997. www.geol.uni-erlangen.de
48. Sherriff, B.L., Grundy, H.D., Hartmann, J.S., Hawthorne, F.C., Cerny, P.: Can. Miner. **29**, 271–285 (1991)

49. Sherriff, B.L., Grundy, H.D., Hartmann, J.S.: Eur. J. Miner. **3**, 751–768 (1991)
50. Mägi, M., Lippma, E., Samoson, A.: J. Phys. Chem. **88**, 1518 (1984)
51. Petkov, V., Billinge, S.J.L., Shastri, S.D., Himmel, B.: Phys. Rev. Lett. **85**, 3436–3439 (2000)
52. Rowles, M.R.: Ph.D. thesis, Curtin University of Technology, Curtin, Australia, 2004.
53. IZA Structure Commission: Database of Zeolite Structures, 2004. http://www.iza-structure.org/databases/
54. Ernst, H., Fenzke, D., Pfiefer, H.: Ann. Phys. **38**, 257–270 (1981)
55. MacKenzie, K.J.D., Brown, I.W.M., Meinhold, R.H., Bowden, M.E.: J. Am. Ceram. Soc. **68**, 293–297 (1985)
56. Rocha, J.: J. Phys. Chem. B **103**, 9801–9804 (1999)
57. Granizo, M.L., Blanco-Varela, M.T., Palomo, A.: J. Mater. Sci. **35**, 6309–6315 (2000)
58. Massiot, D., Bessada, C., Coutres, J.P., Taulelle, F.: J. Magn. Reson. **90**, 231–242 (1990)
59. Kunath-Fandrei, G., Bastow, T.J., Hall, J.S., Jäger, C., Smith, M.E.: J. Phys. Chem. **99**, 15138–15141 (1995)
60. Kunath, G., Losso, P., Schneider, H., Steuernagel, S., Jäger, C.: Solid State Nucl. Magn. Reson. **1**, 261–266 (1992)
61. Kohn, S.C., Dupree, R., Mortuza, M.G., Henderson, C.M.B.: Am. Miner. **76**, 309–312 (1991)
62. Toplis, M.J., Kohn, S.C., Smith, M.E., Poplett, I.J.F.: Am. Miner. **85**, 1556–1560 (2000)
63. Angeli, F., Charpentier, T., Faucon, P., Petit, J.-C.: J. Phys. Chem. B **103**, 10356–10364 (1999)
64. van Aalst, W., den Holander, J., Peterse, W.J.A.M., de Wolff, P.M.: Acta Crystallogr. B **32**, 47–58 (1976)
65. Hanna, J.V., Smith, M.E., Whitfield, H.J.: J. Am. Chem. Soc. **118**, 5772–5777 (1996)
66. Davidovits, J., in: Proceedings of the First International Conference on Alkaline Cements and Concretes, pp. 131–149. Kiev State Technical University, Kiev (1994)
67. Li, Z., Ding, Z., Zhang, Y., in: Wang, K. (ed.) Proceedings of the International Workshop on Sustainable Development and Concrete Technology, pp. 55–76. Iowa State University, Ames, Iowa (2004)
68. Bradley, S.M., Hanna, J.V.: J. Chem. Soc., Chem. Commun. **1993**: 1249–1251 (1993)
69. Bradley, S.M., Hanna, J.V.: J. Am. Chem. Soc. **47**, 7771–7783 (1994)
70. MacMillan, P.W.: Glass Ceramics. Academic Press, London (1964)
71. Meneghini, C., Mobilio, S., Lusvarghi, L., Bondioli, F., Ferrari, A.M., Manfredini, T., Siligardi, C.: J. Appl. Crystallogr. **37**, 890–900 (2004)
72. Mandal, S., Chakrabarti, S., Ghatak, S., Das, S.K.: Bull. Mater. Sci. **28**, 437–443 (2005)
73. Xia, F., Zhang, X., Ren, J., Chen, G., Ma, H., Adam, J.L.: J. Am. Ceram. Soc. **89**, 2154–2157 (2006)

Authors' address: John V. Hanna, NMR Facility, Institute of Materials and Engineering Science, Lucas Heights Research Laboratories, Australian Nuclear Science and Technology Organisation, Private Mail Bag 1, Menai NSW 2234, Australia
E-mail: jvh@ansto.gov.au